Gas Phase Metal Chalcogenide Cluster Ions: A New $[Co_xS_y]^-$ Series Up to $[Co_{38}S_{24}]^-$ and Two $[Fe_xS_y]^-$ Series

John El Nakat, Keith J. Fisher,* Ian G. Dance,* and Gary D. Willett

School of Chemistry, University of New South Wales, PO Box 1, Kensington, NSW 2033, Australia

Received September 18, 1992

Laser (1064 nm) ablation of CoS yields 83 gaseous ions $[Co_xS_y]^-$, detected and characterized by FTICR mass spectrometry. These ions, ranging in size from $[CoS_2]^-$ to $[Co_{38}S_{24}]^-$, possess a slightly curved composition distribution on the x/y plot, with $x/y \sim 1.6$. The same technique applied to FeS and $KFeS_2$, yields 45 $[Fe_xS_y]^-$ ions, which are distributed in two distinct regions of the x/y composition map. Series a is a linear progression of triplets of ions with the compositions $[Fe_nS_{n-1}]^-$, $[Fe_nS_n]^-$, and $[Fe_nS_{n+1}]^-$, for $n = 3$–10, while ions in the unprecedented series b contain an additional S_5, namely $[Fe_nS_{n+5}]^-$ and $[Fe_nS_{n+6}]^-$, for $n = 1$–7. Ions in series a are probably globular clusters, while each ion in series b could contain an additional chelating polysulfide ligand or could evince a structural principle of extended chains or ribbons of linked tetrahedra. Collisionally activated dissociation measurements for the smaller ions reveal stability for $[Fe_6S_6]^-$, $[Co_5S_5]^-$, and $[Co_3S_3]^-$. Cluster structures are postulated for representative ions throughout the composition range. Although there are analogies between probable gas-phase structures of the clusters and core structures for clusters in crystals, the much greater range and number of compositions observed for gaseous clusters presage possibilities for synthesis of new and unexpected clusters in condensed phases. Electronic structures are considered in comparison with those of $[Ni_xS_y]^-$ and $[Cu_xS_y]^-$, revealing that the valence electron population per metal is largely independent of the metal identity, and decreases from about 15 at $x = 5$ to about 12.5 for clusters with 37 metal atoms. This is consistent with increased concentration of metal atoms and metal–metal bonding in the cores of larger clusters.

Introduction

We report new collections of cobalt and iron sulfide clusters, generated as monoanions $[Fe_xS_y]^-$ and $[Co_xS_y]^-$ in the gas phase by laser ablation. The compositions of the $[Fe_xS_y]^-$ ions occur as two distinct populations with no intermediate ions, a characteristic unprecedented in gas phase metal cluster chemistry. The clusters we describe are possibly relevant to all of the frontiers and applications of metal chalcogenides,[1–4] including semiconductor materials,[5] photoresponsive nanoclusters and quantum dots,[6] electrooptic and nonlinearly optic compounds,[7] and biomineralization[8] and to the active site of the enzyme nitrogenase and compounds which model it.[9]

Recent years have seen a renaissance in gas-phase inorganic and cluster chemistry, driven by the major advances in mass spectrometry and ionization techniques.[10,11] The technique we use to obtain new metal sulfide clusters is laser ablation (LA), coupled with Fourier transform ion cyclotron resonance (FTICR) mass spectrometry for characterization. Laser ablation is now well established for the generation of gaseous clusters of metals and nonmetallic elements.[12] Similarly, FTICR mass spectrometric techniques are invaluable for post-detection characterization of these ionized clusters, because the ions can be trapped, separated, and stored in the FTICR cell for some time, during which time it is possible to monitor their fragmentation on collision with inert gases and their reactions with any volatile reactant.[11a,13]

Gas-phase metal oxide clusters have been generated and studied by a variety of methods.[11a,14–17] Metal sulfide chemistry in the

(1) Muller, A., Krebs, B., Eds. *Sulfur, its Significance for Chemistry, for the Geo-, Bio- and Cosmosphere and Technology*; Studies in Inorganic Chemistry 5; Elsevier: Amsterdam, 1984.
(2) Stucky, G. D. Clusters and Cluster-Assembled Materials. *Mater. Res. Soc. Symp. Proc.* **1991**, *206*, 507–520.
(3) Steigerwald, M. L.; Brus, L. E. *Annu. Rev. Mater. Sci.* **1989**, *19*, 471–495.
(4) Averback, R. S.; Bernholc, J.; Nelson, D. L. *Clusters and Cluster Assembled Materials*; Materials Research Society: Pittsburgh, PA, 1991.
(5) Jarrold, M. F. Metal and Semiconductor Cluster Ions. In Russell, D. H. *Gas Phase Inorganic Chemistry*; Russell, D. H., Ed.; Plenum Press: New York, 1989; Chapter 5, pp 137–192.
(6) (a) Henglein, A. *Chem. Rev.* **1989**, *89*, 1861–1873. (b) Wang, Y.; Herron, N. *J. Phys. Chem.* **1991**, *95*, 525–532. (c) Spanhel, L.; Hasse, M.; Weller, H.; Henglein, A. *J. Am. Chem. Soc.* **1987**, *109*, 5649–5655. (d) Variano, B. F.; Hwang, D. M.; Sandroff, C. J.; Wiltzius, P.; Jing, T. W.; Ong, N. P. *J. Phys. Chem.* **1987**, *91*, 6455–6458. (e) Wang, Y.; Mahler, S. W.; Kasowski, R. *J. Chem. Phys.* **1987**, *87*, 7315–7322. (f) Nozik, A. J.; Williams, F.; Nenadovic, M. T.; Rajh, T.; Micic, O. I. *J. Phys. Chem.* **1985**, *89*, 397–399.
(7) (a) Wang, Y.; Mahler, W.; Herron, N. *J. Opt. Soc. Am.* **1989**, *B6*, 808. (b) Cheng, L-T.; Herron, N.; Wang, Y. *J. Appl. Phys.* **1989**, *66*, 3417–3419.
(8) (a) Dameron, C. T.; Reese, R. N.; Mehra, R. K.; Kortan, A. R.; Carroll, P. J.; Steigerwald, M. L.; Brus, L. E.; Winge, D. R. *Nature* **1989**, *338*, 596–597. (b) Dameron, C. T.; Smith, B. R.; Winge, D. R. *J. Biol. Chem.* **1989**, *264*, 17355–17360. (c) Dameron, C. T.; Winge, D. R. *Inorg. Chem.* **1990**, *29*, 1343–1348.
(9) (a) Berg, J. M.; Holm, R. H. In *Iron-Sulfur Proteins*; Spiro, T. G., Ed.; Wiley-Interscience: New York, 1982; Vol. 4, Chapter 1. (b) Coucouvanis, D. *Acc. Chem. Res.* **1991**, *24*, 1. (c) Holm, R. H.; Ciurli, S.; Weigel, J. A. *Prog. Inorg. Chem.* **1990**, *38*, 1 and references cited therein.
(10) Russell, D. H. *Gas Phase Inorganic Chemistry*; Plenum Press: New York, 1989; p 412.
(11) (a) Irion, M. P.; Selinger, A.; Wendel, R. *Int. J. Mass Spectrom. Ion Processes* **1990**, *96*, 27–47. (b) Bernstein, E. R. *Studies Phys. Theor. Chem.* **1990**, *68*, 806. (c) Eller, K.; Schwarz, H. *Chem. Rev.* **1991**, *91*, 1121–1177.
(12) Lubman, D. M. *Lasers and Mass Spectrometry*; Oxford University Press: London, 1990.
(13) (a) Comisarow, M. B. *Adv. Mass Spectrom.* **1980**, *8*, 1698. (b) Wanczek, K. P. *Int. J. Mass Spectrom. Ion Processes* **1984**, *60*, 11. (c) Gross, M. L.; Renpel, D. L. *Science* **1984**, *226*, 261. (d) Freiser, B. S. In *Techniques in Ion Molecule Reactions*, Farrar, J. M., Saunders, W. H., Eds.; Wiley: New York, 1989; pp 61–118. (e) Marshall, A. G. *Acc. Chem. Res.* **1985**, *18*, 316. (f) Wilkins, C. L.; Chowdhury, A. K.; Nuwaugir, L. M.; Coates, M. L. *Mass Spectrom. Rev.* **1989**, *8*, 67. (g) Russell, D. H. *Mass Spectrom. Rev.* **1986**, *5*, 167. (h) Marshall, A. G. *Adv. Mass Spectrom.* **1989**, *11A*, 651–668. (i) Sharpe, P.; Richardson, D. E. *Coord. Chem. Rev.* **1989**, *93*, 59. (j) Irion, M. P.; Selinger, A.; Wendel, R. *Int. J. Mass Spectrom. Ion Processes* **1990**, *96*, 27. (k) Marshall, A. G.; Verdun, F. R. In *Fourier Transforms in NMR, Optical and Mass Spectrometry, a Users Handbook*; Elsevier: Amsterdam, 1989.
(14) (a) Gord, J. R.; Bemish, R. J.; Freiser, B. S. *Int. J. Mass Spectrom. Ion Processes* **1990**, *102*, 115–132. (b) Mele, A.; Consalvo, D.; Stranges, D.; Giardini-Guidoni, A.; Teghil, R. *Int. J. Mass Spectrom. & Ion Processes* **1990**, *95*, 359–373. (c) Fisher, E. R.; Elkind, J. L.; Clemmer, D. E.; Georgiadis, R.; Loh, S. K.; Aristov, N.; Sunderlin, L. S.; Armentrout, P. B. *J. Chem. Phys.* **1990**, *93*, 2676–91. (d) Maleknia, S.; Brodbelt, J.; Pope, K. *J. Am. Soc. Mass Spectrom.* **1991**, *2*, 212. (e) Fisher, K. J.; Smith, D. R.; Willett, G. D. *Proceedings of the 39th ASMS Conference on Mass Spectrometry and Allied Topics*; ASMS: Nashville, TN, 1991; p 37.

0020-1669/93/1332-1931$04.00/0

gas phase is less well understood. Subsequent to some early work[18-20] using classical mass spectrometric and vaporization techniques on metal chalcogenide compounds, Freiser et al. have examined the ions $[MS_y]^+$ (M = Fe, Co, V, Ti; y = 1–8) formed by reaction of M^+ with ethylene sulfide,[21] while Parent[22] has observed sixteen $[Al_xS_y]^+$ clusters up to $[Al_7S_{10}]^+$ by LA–FTICR of Al_2S_3. Martin[23] reports $[As_xS_y]^+$ clusters and Schild et al.[24] report $[Pb_xE_y]^+$ (E = Se, Te) clusters, formed in both cases by thermal evaporation. Linton et al.[25] have demonstrated the formation of small $[Ni_xS_y]^+$ ions by laser ablation of NiS. Attempts to deposit clusters formed by laser evaporation of FeS_2 in helium yielded only FeS.[26]

Our previous reports of gaseous metal chalcogenide cluster ions formed by laser ablation have covered nickel, copper, and silver. The nickel sulfides NiS and Ni_3S_2 yielded a series of 27 negative ions $[Ni_xS_y]^-$, ranging in size from $[NiS]^-$ to $[Ni_{15}S_{10}]^-$.[27] Laser ablation of various solid copper chalcogenide compounds, and of mixtures of Cu with Se or Te, yielded collections of anions $[Cu_xE_y]^-$ (E = S, Se, Te) ranging in size up to $[Cu_{45}S_{23}]^-$ and demonstrating a dominant series in which $x = 2y - 1$.[28] In a similar investigation with silver chalcogenides, the most intense large ions also follow the general progression $[Ag_{2y-1}E_y]^-$ up to $y = 11$.[29]

In this paper we describe our LA–FTICR experiments on FeS, $KFeS_2$, and CoS. Under our conditions CoS yields more clusters in the class $[M_xS_y]^-$ than any other metal chalcogenide investigated so far. The iron compounds yield two series of $[Fe_xS_y]^-$ clusters, distinctly separate in composition, which we believe represent different structural principles.

Experimental Section

The FeS used was the commercial solid, while the $KFeS_2$ was prepared by the fusion method.[30] Since the spectra are largely independent of the sample composition, low grade samples can be used. Our LA–FTICR technique does not at this stage use an external ion source, and therefore ferromagnetic iron sulfide samples have not been investigated. CoS was prepared by the reaction of aqueous cobalt nitrate solution with H_2S and was washed and dried in vacuum.

Mass spectra were obtained from pressed samples as previously reported,[27] using a Spectrospin CMS-47 FT-ICR mass spectrometer, equipped with a 4.7-T magnet. Ion generation by laser ablation used a Nd-YAG laser (1064 nm, Spectra Physics DCR-11) focused to an area of 0.1 mm^2. In the Q-switched mode the pulse width was 8 ns and the laser power was varied between 5 and 56 mJ using neutral density filters. Time delays ranging from 0.005 to 0.1 s were introduced between the laser pulse and the measurement of the FTICR spectra and caused some variation in the relative intensities of the ions due to the varying periods for gas-phase reactions and formation of clusters.

Narrow-band and high-resolution spectra were used to identify ions up to m/z 1800. As cobalt is monoisotopic and sulfur and iron have one isotope in large abundance, the ions are reported with the mass of the major peak.

In the collisional activation experiments the ion of interest was generated by the laser pulse and allowed to relax in the collision gas argon at 1×10^{-7} mbar, for periods of 0.1–1 s. Then all other ions were ejected from the cell, and the remaining ion was activated by an rf pulse of between 30 and 100 μs. After collisional activation for 0.01–0.1 s, the product ions were excited and observed.

Results

The positive ion spectra of FeS and $KFeS_2$ and of CoS were dominated by the naked metal ion M^+ and contained only a few metal sulfide ions of small mass and low intensity. In contrast, prolific negative ion spectra were readily obtained from all samples. Figure 1 shows part of the broadband negative ion spectrum of $KFeS_2$, while Table I lists the ions and their relative intensities when obtained from $KFeS_2$ and FeS. Ions up to $[Fe_{10}S_9]^-$ have been identified by high resolution measurements, while ions with m/z >900 were very weak and could not be identified unambiguously. Attempts to investigate FeSe were thwarted by the ferromagnetism of the sample. Figure 2 shows a broadband LA FTICR negative ion spectrum of CoS, starting at m/z 500, with $[Co_xS_y]^-$ ions extending up to m/z 3100. The base peak for CoS was $[Co_3S_3]^-$ (not shown in Figure 2), while $[CoS]^-$ was not observed. Using the high-resolution mode it has been possible to assign unambiguously the compositions of the ions ranging up to m/z 1776 ($[Co_{22}S_{15}]^-$), and these ions are listed with their relative intensities in Table II. At masses higher than m/z 1780, the decreasing intensities of the ions preclude the good narrow band spectra that would be required for unambiguous assignment. However there is little doubt about the assigned compositions of most of them. They progress in a pattern similar to that shown by the ions identified unequivocally. It can be noted that in the progression of $[Co_xS_y]^-$ up to m/z ~3000 there are in general two values of y for each value of x: for example the last four ions identified are $[Co_{37}S_{23}]^-$, $[Co_{37}S_{24}]^-$, $[Co_{38}S_{23}]^-$, and $[Co_{38}S_{24}]^-$.

The details of the ion distributions are dependent on the laser power, and on the delay between the laser pulse and the measurement of the mass spectrum. For both metals, higher power yields larger ions, and longer delays decrease the relative abundances of the larger ions. Spectra for CoS observed at maximum laser power (56 mJ) contained more ions at high mass (m/z >1400) than the spectra observed at lower laser powers. Delays of 0.005–0.01 s between the laser pulse and acquisition gave spectra with more abundant high mass ions with m/z >1400, while delays greater than 0.01 s gave spectra with low intensity for ions with m/z >1400 and greater relative intensity of ions with m/z <600.

One technique we have used to seek information on the origins and formation of the ions involves modification of the composition and structure of the precursor solid ablated. For iron the ions generated are largely independent of the composition of the sample, with FeS and $KFeS_2$ yielding almost the same collection of negative ions. Unfortunately due to the volatility of elemental sulfur and the magnetism of the metal, it has not been possible to undertake LA experiments with mixtures of the elements (Fe or Co with S_8) in our FTICR cell, as has been achieved for copper and silver with selenium and tellurium.[28,29] Evidently a plasma containing a large set of negative ions is formed on laser ablation of iron or cobalt sulfides, with masses ranging up to m/z 3000.

(15) (a) King, F. L.; Parent, D. C.; Ross, M. M. *J. Chem. Phys.* **1991**, *94*, 2578. (b) Parent, D. C. *Chem. Phys. Lett.* **1991**, *183*, 51–54.
(16) Radi, P. P.; von Helden, G.; Hsu, M.-T.; Kemper, P. R.; Bowers, M. T. *Int. J. Mass Spectrom. Ion Processes* **1991**, *109*, 49–73.
(17) (a) Sone, Y.; Hoshino, K.; Naganuma, T.; Nakajima, A.; Kaya, K. *J. Phys. Chem.* **1991**, *95*, 6830–6832. (b) Nakajima, A.; Kishi, T.; Sugioka, T.; Sone, Y.; Kaya, K. *J. Phys. Chem.* **1991**, *95*, 6833–6835.
(18) (a) Goldfinger, P.; Jeunehomme, M. *Trans. Farad. Soc.* **1963**, *59*, 2851–2867. (b) De Maria, G.; Goldfinger, P.; Malaspina, L.; Piacente, V. *Trans. Farad. Sci.* **1965**, *61*, 2146–2152.
(19) (a) Colin, R.; Drowart, J. *J. Chim. Phys.* **1962**, *37*, 1120–1121. (b) Coppens, P.; Smoes, S.; Drowart, J. *Trans. Farad. Soc.* **1967**, *63*, 2140–2147. (c) Colin, R.; Drowart, J. *Trans. Farad. Soc.* **1968**, *64*, 2611–2621. (d) Uy, O. M.; Drowart, J. *Trans. Farad. Soc.* **1968**, *65*, 3221–3230.
(20) Uy, O. M.; Muenow, D. W.; Ficalora, P. J.; Margrave, J. L. *Trans. Farad. Soc.* **1968**, *64*, 2998–3005.
(21) (a) Carlin, T. J.; Wise, M. B.; Freiser, B. S. *Inorg. Chem.* **1981**, *20*, 2745. (b) MacMahon, T. J.; Jackson, T. C.; Freiser, B. S. *J. Am. Chem. Soc.* **1989**, *111*, 421–427.
(22) Parent, D. C. *Chem. Phys. Lett.* **1991**, *183*, 45–50.
(23) Martin, T. P. *J. Chem. Phys.* **1984**, *80*, 170–175.
(24) Schild, D.; Pflaum, R.; Riefer, G.; Recknagel, E. *Z. Phys. D* **1988**, *10*, 329–335.
(25) (a) Musselman, I. H.; Linton, R. W.; Simons, D. S. *Anal. Chem.* **1988**, *60*, 110. (b) Linton, R. W.; Musselman, I. H.; Bruynseels, F.; Simons, D. S. In *Microbeam Analysis*, Geiss, R. H., Ed.; San Francisco Press: San Francisco, CA, 1987; p 365.
(26) Faust, P.; Brandstattner, M.; Ding, A. *Z. Phys.* **1991**, *21*, 285–288.
(27) El Nakat, J. H.; Dance, I. G.; Fisher, K. J.; Rice, D.; Willett, G. D. *J. Am. Chem. Soc.* **1991**, *113*, 5141–5148.
(28) El Nakat, J. H.; Dance, I. G.; Fisher, K. J.; Willett, G. D. *Inorg. Chem.* **1991**, *30*, 2957–2958.
(29) El-Nakat, H. J.; Dance, I. G.; Fisher, K. J.; Willett, G. D. *J. Chem. Soc., Chem. Commun.* **1991**, 746–748.
(30) Bronger, W. *Z. Anorg. Allg. Chem.* **1968**, *359*, 225–233.

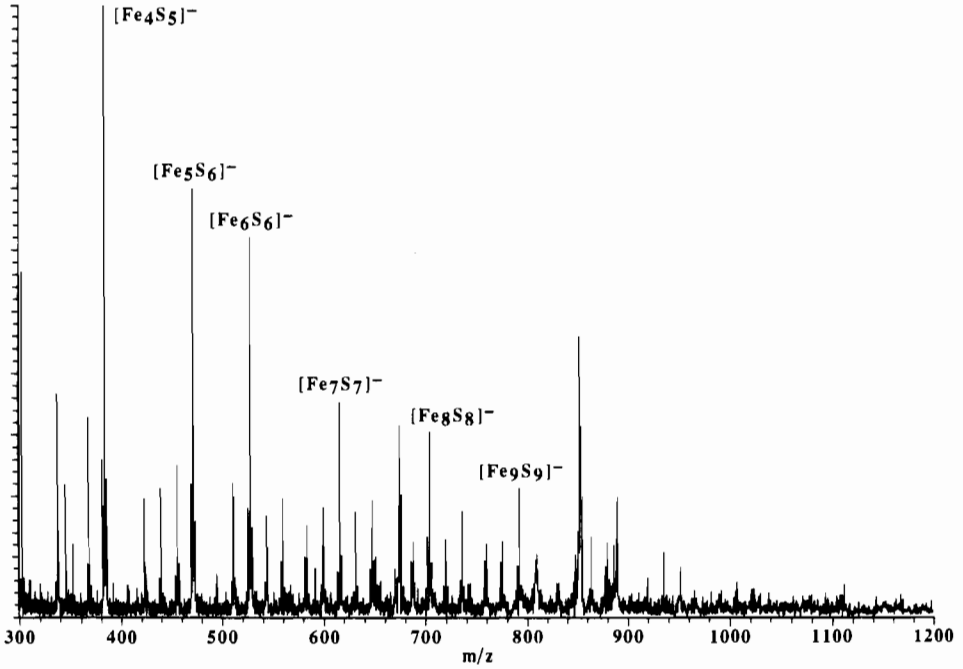

Figure 1. Broad-band negative ion mass spectrum of laser-ablated $KFeS_2$. Selected ion compositions are labeled; the peak at m/z 850 is an artifact.

Collisionally Activated Dissociation. The products of the dissociation of the $[Fe_xS_y]^-$ and $[Co_xS_y]^-$ clusters after activation and collision with argon are presented in Table III. These experiments were possible only with ions of sufficient intensity, and therefore results are available only for the more intense smaller ions. We were generally able to observe one or two daughter ions, except in the few cases where dissociation did not occur. These daughter ions were observed within <0.1 s; other ions were observed at longer times, as indicated in Table III. The ion $[Fe_2S_3]^-$ yields $[FeS_2]^-$ as daughter, with loss of neutral FeS. $[FeS_2]^-$ is also observed as a major ion from solid FeS, and is evidently stable. $[Fe_3S_3]^-$ dissociates to produce $[Fe_2S_3]^-$ with loss of Fe; there is no evidence on whether $[Fe_2S_3]^-$ as daughter of $[Fe_3S_3]^-$ is the same as $[Fe_2S_3]^-$ formed directly. $[Fe_3S_4]^-$ undergoes relatively minor fragmentation to Fe_3S_3 and S, with the negative charge distributed both ways. $[Fe_4S_5]^-$ dissociates by loss of neutral Fe_3S_3 leaving $[FeS_2]^-$; the more probable structures for these, consistent with this dissociation, are discussed below. $[Fe_5S_6]^-$ and $[Fe_6S_6]^-$ are relatively stable, with the ions $[Fe_3S_3]^-$ and $[Fe_3S_4]^-$ and the neutrals Fe, FeS_2, Fe_2S, Fe_3S_3, and Fe_4S_4 as relatively minor products. We use this information below in proposing probable structures for these ions. The dissociations of the $[Co_xS_y]^-$ ions frequently involve the loss of the neutrals Co, CoS, Co_2S, and S_2. The absence of $[CoS]^-$ and the prevalence of CoS indicates that CoS has low electron affinity. The limited dissociation of $[CoS_2]^-$ and its formation as an abundant daughter of $[Co_2S_3]^-$ is consistent with a stable structure, probably linear. We note that $[Co_3S_3]^-$ is the most intense ion in the spectrum of CoS and is also a common product of dissociation of other ions: it is evidently stable. Other frequently appearing ions are $[Co_4S_2]^-$ and $[Co_6S_4]^-$.

Long reaction times generally lead to reaction products such as S_3 and S, which can undergo ion–molecule reactions with other species in the cell. As an illustration, Co_4S_5 was observed after long collisional activation of Co_5S_4 (with less S), probably through the sequence

$$Co_5S_4 - Co \rightarrow Co_4S_4 + S \rightarrow Co_4S_5$$

Patterns of Ion Compositions. The distributions of compositions for the ions are displayed in the ion maps shown in Figures 3 (for Fe) and 4 (for Co). An unprecedented result occurs for the ions $[Fe_xS_y]^-$ which fall into two distinct and well-defined series on the ion map. Series a is a linear progression of triplets of ions with the compositions $[Fe_nS_{n-1}]^-$, $[Fe_nS_n]^-$, and $[Fe_nS_{n+1}]^-$, for n = 1–10 (with a few members missing at each end of the series). The second, series b, is a complete series of doublets of ions $[Fe_nS_{n+5}]^-$ and $[Fe_nS_{n+6}]^-$, for n = 1–7. The ions in series b are unusually sulfur rich, containing S_5 additional to the ions in series a, and it is tempting to postulate that they contain polysulfide chains. However these sulfur-rich ions are different from the $[FeS_y]^+$ polysulfide cations described by Freiser.[21b] There is one sulfur-rich ion, $[Fe_2S_6]^-$, which is observed in addition to those described by series b. The sulfur-rich ions are more prevalent in the ablation of FeS than $KFeS_2$, despite the higher S/Fe ratio in the latter: FeS is known to undergo surface oxidation, generating polysulfides, but we were not able to confirm this for our samples.

The map of $[Co_xS_y]^-$ ions, shown in Figure 4, is generally two or three ions wide up to x = 20; that is in this range there are two or three values of y for each x and two or three values of x for each y. In the higher mass region the distribution of ions develops zigzag characteristics, such that successive increments involve atoms of the same type. Thus clusters after $[Co_{26}S_{15}]^-$ can be described by addition mainly of S atoms up to $[Co_{28}S_{21}]^-$, after which there is an increase mainly by Co addition up to $[Co_{33}S_{22}]^-$; these statements reflect structure concepts, without implications for growth processes or mechanisms. The overall distribution of $[Co_xS_y]^-$ ions is about a line curving slightly toward increased proportions of Co atoms as the size of the cluster increases.

Discussion

As in the laser ablation of other metal chalcogenides,[27–29] few relatively small positive ions (mainly M^+ and S_n^+) are formed by high powered laser ablation of iron and cobalt sulfides. The formation of positive ions is the result of multiphoton ionization when a large amount of energy is delivered to the sample in a short time.

The large numbers of negative ions produced by all samples suggest that their formation is by a process different from that for the positive ions. The ablation need not form negative ions directly, but could generate a large collection of neutral clusters, and free electrons; electron capture by neutral species with high electron affinity could be responsible for the population of negative

Table I. Negative Ions Observed from the Laser Ablation of $KFeS_2$ and FeS

ion	mass	rel intens $KFeS_2$	rel intens FeS
S_3	96	100	61
FeS_2	120	9	100
S_4	128	50	18
FeS_3	152	4	4
S_5	160	35	20
Fe_2S_2	176	0[a]	6
S_6	192	48	9
Fe_2S_3	208	6	19
Fe_3S_2	232	0[a]	7
FeS_6	248	0[a]	30
Fe_3S_3	264	13	42
FeS_7	280	0[a]	16
Fe_3S_4	296	13	25
Fe_2S_6	304	0[a]	8
Fe_4S_3	320	0[a]	19
Fe_2S_7	336	2	20
Fe_4S_4	352	3	29
Fe_2S_8	368	7	32
Fe_4S_5	384	23	19
Fe_5S_4	408	2	5
Fe_3S_8	424	6	13
Fe_5S_5	439	5	22
Fe_3S_9	456	7	21
Fe_5S_6	472	19	11
Fe_6S_5	495	2	7
Fe_4S_9	511	6	17
Fe_6S_6	527	15	16
Fe_4S_{10}	544	4	6
Fe_6S_7	559	6	0[a]
Fe_7S_6	583	4	6
Fe_5S_{10}	599	4	5
Fe_7S_7	615	10	6
Fe_5S_{11}	632	5	3
Fe_7S_8	647	6	6
Fe_8S_7	671	3	0[a]
Fe_6S_{11}	687	4	0[a]
Fe_8S_8	703	9	6
Fe_6S_{12}	719	4	0[a]
Fe_8S_9	735	4	0[a]
Fe_9S_8	759	3	5
Fe_7S_{12}	775	3	3
Fe_9S_9	791	3	4
Fe_7S_{13}	807	2	3
$Fe_{10}S_9$	847	6	3
Fe_8S_{13}	863	2	3
$Fe_{10}S_{10}$[b]	879	2	2
Fe_9S_{12}[b]	887	3	0[a]
Fe_9S_{13}[b]	919	1	3
$Fe_{11}S_{10}$[b]	935	2	3

[a] Not observed. [b] Insufficient intensity for confirmation by high resolution.

ions observed. An experiment in which the cell was flooded with electrons caused no changes in the spectrum, but this could indicate simply that ablation generates a sufficient electron flux.

The large number of high-mass negative ions produced from CoS is unprecedented. The spectrum in Figure 2 is much richer than any produced by the other metal chalcogenides we have investigated. Laser ablation of CuS, Cu_2S, and KCu_4S_3 yields $[Cu_xS_y]^-$ clusters to higher mass (m/z 3600)[28] than observed for $[Co_xS_y]^-$ clusters from CoS, but the $[Co_xS_y]^-$ spectrum contains many more ions than does the $[Cu_xS_y]^-$ spectrum.

An entirely unexpected and unprecedented result is the occurrence of $[Fe_xS_y]^-$ ions in two well-defined linear series, which are clearly separated from each other on the ion map (Figure 3) by a composition region in which no ions are observed. Because series a contains triplets of ions $[Fe_nS_{n-1}]^-$, $[Fe_nS_n]^-$, and $[Fe_nS_{n+1}]^-$ and series b contains $[Fe_nS_{n+5}]^-$ and $[Fe_nS_{n+6}]^-$, the increment of sulfur atoms in the polysulfide series ions is 4, 5, 6, or 7. It is significant that no ions with increments of S_2 or S_3 are observed; there is evidently special stability associated with S_5 and S_6. Since it is now well established in polychalcogenide chemistry[31-33] that stable metal complexes exist (in crystals and solutions) with chelating polysulfide ligands most commonly containing four, five, or six sulfur atoms in the MS_m chelate, there is an obvious interpretation that the ions in series b contain FeS_5 or FeS_6 chelates. Such polysulfide incrementation is precisely defined (implying stability) but can be invoked only once per cluster ion because there is no evidence of ions of the type $[Fe_nS_{n+10}]^-$.

Iron polychalcogenide chemistry in the solid state demonstrates two complexes, $[(E_5)Fe(\mu\text{-}E)_2Fe(E_5)]^2$ (E = S, Se),[34] which contain bidentate polychalcogenide and bridging chalcogenide ions. We note that in the laser ablation spectrum of FeS, $[FeS_6]^-$ with m/z 248 is one of the more intense ions; it is possible that this is $[Fe_2S_{12}]^{2-}$, with the same structure as the solid complexes. Freiser et al.[21b] have reported different positive sulfur-rich iron ions in the gas phase, namely $[FeS_n]^+$ n = 1–6, formed through reactions $[FeS_{n-1}]^+ + C_2H_4S \rightarrow [FeS_n]^+ + C_2H_4$. The compositions, photodissociations, CID products, and ion-molecule reactions of these $[FeS_n]^+$ ions indicate that they contain S_2, S_3, and S_4 units. Comparable data on our negative ions, from collisionally activated dissociation experiments, are available only for the smallest members of series b, $[FeS_6]^-$ and $[FeS_7]^-$, where S_2 loss was apparent. Disulfide and trisulfide ligands coordinated to Fe are known in crystalline compounds,[35] and the mineral pyrites contains disulfide.

The polysulfide chain interpretation is not the only hypothesis for the structures of the ions in series b; others are developed below after discussion of the probable structures of the ions in series a.

Structures of the $[M_xS_y]$ Clusters. We develop here structural postulates for many of the observed $[M_xS_y]^-$ ions, using the following guidelines: (i) recurring structural features which are confirmed by diffraction methods in related metal chalcogenide compounds are used as structural paradigms; (ii) it is assumed that the structures of the clusters (which have been thermalized) are approximately globular; (iii) it is assumed that structures with peripherally exposed M atoms would be less stable than those with peripheral S atoms; (iv) it is assumed that the more stable structures maximize the number of M–S and M–M bonding connections. After posulation of the models according to these principles, each of them has been developed geometrically by computer optimization of bond distances to values of 2.2 Å for M–S and 2.5 Å for M–M. [Our preliminary calculations by density functional methods yield slightly shorter distances, but postulation of models for the cores relies on the ratio of M–M to M–S bond distances, not absolute values.] The models are presented as the most reasonable postulates for the structures of the gas-phase clusters, that is as the models to be refined by calculations of electronic structure: these calculations are in progress. Throughout this paper structures for $[M_xS_y]^-$ clusters are labeled ***xy*X**, where X = A, B, ..., for different structure postulates for one composition. We recognize that there could be structural isomers for these ions and that ions of the same composition but formed differently, such as by dissociation or association, can have different structures and reactivities.

(31) (a) Banda, R. M. H.; Dance, I. G.; Bailey, T. D.; Craig, D. C.; Scudder, M. L. *Inorg. Chem.* **1989**, *28*, 1862–1871. (b) Bailey, T. D.; Banda, R. M. H.; Craig, D. C.; Dance, I. G.; Ma, I. N. L. *Inorg. Chem.* **1991**, *30*, 187–191. (c) Banda, R. M. H.; Craig, D. C.; Dance, I. G.; Scudder, M. L. *Polyhedron* **1989**, *8*, 2379–2383.
(32) Ansari, M. A.; Ibers, J. A. *Coord. Chem. Rev.* **1990**, *100*, 223–266.
(33) Kanatzidis, M. G. *Comments Inorg. Chem.* **1990**, *10*, 161–195.
(34) (a) Coucouvanis, D.; Swenson, D.; Stremple, P.; Baenziger, N. C. *J. Am. Chem. Soc.* **1979**, *101*, 3392. (b) Strasdeit, H.; Krebs, B.; Henkel, G. *Inorg. Chim. Acta* **1984**, *89*, L11–L13.
(35) (a) Vergamini, P. J.; Ryan, R. R.; Kubas, G. J. *J. Am. Chem. Soc.* **1976**, *98*, 1980. (b) Kubas, G. J.; Vergamini, P. J. *Inorg. Chem.* **1981**, *20*, 2667–2676. (c) Müller, A.; Schladerbeck, N. *Chimia* **1985**, *39*, 23–24. (d) Dev, S.; Ramli, E.; Rauchfuss, T. B.; Wilson, S. R. *Inorg. Chem.* **1991**, *30*, 2514–2519.

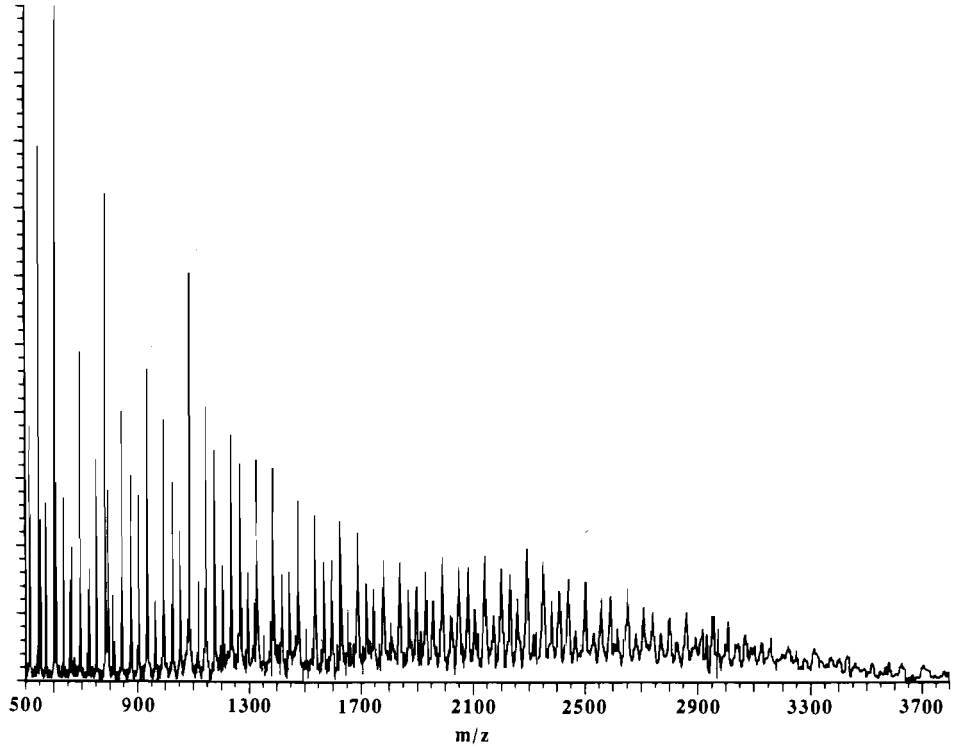

Figure 2. Broad-band negative ion mass spectrum of laser-ablated CoS.

Expected Structural Features for $[Fe_nS_{n-1}]^-$, $[Fe_nS_n]^-$ and $[Fe_nS_{n+1}]^-$ Ions. A considerable number of Fe_xS_y cores in heteroligated clusters is now known.[36] Representative structures for these cores are linear Fe_3S_4, cubanoid Fe_4S_4, hexagonal prismatic Fe_6S_6,[37] Fe_6S_6 with basket topology,[38] planar Fe_6S_9,[39] monocapped hexagonal prismatic Fe_7S_6,[38a,38d,40] and cubic Fe_8.[41] All of these have terminal heteroligands, but there are three larger structures without terminal ligands, namely monocyclic $[\alpha\text{-}Na_2Fe_{18}S_{30}]^{8-}$,[36] monocyclic $[\beta\text{-}Na_2Fe_{18}S_{30}]^{8-}$,[36c] and bicyclic $[Na_9Fe_{20}Se_{38}]^{9-}$.[36c] All of the many compounds with Fe_xS_y cores possess a common structural feature, which is the existence of Fe_2S_2 rhombs, fused in various ways in the different structures. Holm[36] has drawn attention to this structural paradigm, in which Fe–Fe bonding interactions are generally present.

We propose that the same core structural features occur in the gas phase $[Fe_xS_y]^-$ clusters in series a. A selection of the postulated structures is presented in Figure 5. The fact that $y = x$ or $y = x \pm 1$ in these ions means that structures built from FeS pairs or Fe_2S_2 rhombs are logical, and it also means that the average coordination numbers of Fe and S are the same. It is generally impossible to have 4-fold coordination of both Fe and S, and in general the average coordination numbers of one atom type by the other type are closer to 3. Some postulated structures have only two S per Fe, but in these there are compensating Fe–Fe bonds.

The most symmetrical structure type for $[Fe_2S_3]^-$ has three S atoms bridging the two Fe atoms, $(\mu\text{-}S)_3Fe_2$ (**23A**); this does not however account easily for its dissociation to $[FeS_2]^-$ and FeS. There are three structural isomers for $[Fe_3S_3]^-$, namely $(\mu\text{-}S)_3Fe_3$ (**33A**), $(\mu_3\text{-}S)(\mu\text{-}S)_2Fe_3$ (**33B**), and $(\mu_3\text{-}S)_2(\mu\text{-}S)Fe_3$ (**33C**). In view of the fragmentation of $[Fe_3S_3]^-$ to $[Fe_2S_3]^-$ with loss of Fe, we postulate structure **33C** as the most likely for $[Fe_3S_3]^-$, yielding **23A**. Structures **34A** and **43A** (both not shown) are voided cubanes, that is **44A** with Fe or S removed. Cubanoid clusters are well-known in condensed phases and could be expected for the gas phase ions. Evidence for the stability of cubanoid topologies is found in the limited collisional activation of $[Fe_3S_4]^-$ and the appearance of $[Fe_3S_4]^-$ and Fe_4S_4 as daughters of larger ions. For $[Fe_4S_5]^-$ a model with S added across a face of **44A** has S atoms crowded on the surface, and we propose instead **45A** for which the observed scission to Fe_3S_3 and $[FeS_2]^-$ is readily conceived. **54A** and the pentacapped square pyramid **55A** are plausible structures for $[Fe_5S_4]^-$ and $[Fe_5S_5]^-$; **55A** is related to **45A**. $[Fe_5S_6]^-$ is an abundant and stable ion, for which we propose structure **56A**.

The $[Fe_6S_6]$ core with various terminal ligands is known to exist as two connectivity isomers in crystals, namely the puckered hexagonal prismane **66A**[37] and the basket core **66B**.[38] Both contain a new structural feature, the Fe_3S_3 cycle. Stereochemical isomers are possible for **66A** according to the degree of Fe–Fe bonding, as for example in **66C**. We can also postulate **66D**, which has fused cubanes and is composed only of Fe_2S_2 rhombs. We believe that the tight structures **66C** and **66D** are most probable for $[Fe_6S_6]^-$, which is a stable ion in the gas phase. For larger ions, a general structure expansion principle that can be applied at this stage involves addition of S to an Fe–Fe diagonal, addition of Fe to an S–S diagonal, or addition of Fe–S to an Fe_3S_3 cycle. Application to **66A** generates **76A** and **67A** (not shown), both of which contain nine Fe_2S_2 rhombs and one Fe_3S_3. The

(36) (a) You, J-F.; Snyder, B. S.; Papefthymiou, G. C.; Holm, R. H. *J. Am. Chem. Soc.* **1990**, *112*, 1067–1076. (b) You, J-F.; Snyder, B. S.; Holm, R. H. *J. Am. Chem. Soc.* **1988**, *110*, 6589–6591. (c) You, J-F.; Papaefthymiou, G. C.; Holm, R. H. *J. Am. Chem. Soc.* **1992**, *114*, 2697–2710.

(37) (a) Kanatzidis, M. G.; Hagen, K. S.; Dunham, W. R.; Lester, R. K.; Coucouvanis, D. *J. Am. Chem. Soc.* **1985**, *107*, 953–961. (b) Kanatzidis, M. G.; Salifoglou, A.; Coucouvanis, D. *Inorg. Chem.* **1986**, *25*, 2460–2468. (c) Coucouvanis, D.; Kanatzidis, M. G.; Salifoglou, A.; Dunham, W. R.; Simopolous, A.; Sams, J. R.; Papaefthymiou, V.; Kostikas, A.; Strouse, C. E. *J. Am. Chem. Soc.* **1987**, *109*, 6863.

(38) (a) Snyder, B. S.; Reynolds, M. S.; Noda, I.; Holm, R. H. *Inorg. Chem.* **1988**, *27*, 595–597. (b) Reynolds, M. S.; Holm, R. H. *Inorg. Chem.* **1988**, *27*, 4494–4499. (c) Snyder, B. S.; Holm, R. H. *Inorg. Chem.* **1990**, *29*, 274–279. (d) Snyder, B. S.; Reynolds, M. S.; Holm, R. H.; Papaefthymiou, G. C.: Frankel, R. B. *Polyhedron* **1991**, *10*, 203–213. (e) Snyder, B. S.; Holm, R. H. *Inorg. Chem.* **1988**, *27*, 2339.

(39) (a) Christou, G.; Sabat, M.; Ibers, J. A.; Holm, R. H. *Inorg. Chem.* **1982**, *21*, 3518. (b) Strasdeit, H.; Krebs, B.; Henkel, G. *Inorg. Chem.* **1984**, *23*, 1816. (c) Hagen, K. S.; Watson, A. D.; Holm, R. H. *J. Am. Chem. Soc.* **1985**, *105*, 3905. (d) Strasdeit, H.; Krebs, B.; Henkel, G. *Z. Naturforsch.* **1987**, *B42*, 565.

(40) Noda, I.; Snyder, B. S.; Holm, R. H. *Inorg. Chem.* **1986**, *25*, 3851.

(41) Pohl, S.; Saak, W. *Angew. Chem., Int. Ed. Engl.* **1984**, *23*, 907. Saak, W.; Pohl, S. *Angew. Chem., Int. Ed. Engl.* **1991**, *30*, 881.

Table II. Negative Ions Observed from the Laser Ablation of CoS[a]

ion	mass	intens	ion	mass	intens
CoS_2	123	49	$Co_{22}S_{15}$	1776	3
Co_2S_2	182	8	$Co_{23}S_{14}$	1803	2
Co_2S_3	214	37	$Co_{23}S_{15}$	1835	4
Co_3S_3	273	100	$Co_{23}S_{16}$	1867	3
Co_4S_4	364	54	$Co_{24}S_{15}$	1894	3
Co_5S_4	423	32	$Co_{24}S_{16}$	1926	4
Co_5S_5	455	17	$Co_{25}S_{15}$	1953	3
Co_6S_4	482	15	$Co_{25}S_{16}$	1985	5
Co_6S_5	514	9	$Co_{26}S_{16}$	2043	4
Co_6S_6	546	20	$Co_{26}S_{17}$	2075	4
Co_7S_5	573	6	$Co_{27}S_{16}$	2102	3
Co_7S_6	605	25	$Co_{27}S_{17}$	2134	5
Co_8S_6	663	5	$Co_{27}S_{18}$	2166	2
Co_8S_7	695	12	$Co_{27}S_{19}$	2198	4
Co_9S_7	754	8	$Co_{28}S_{18}$	2225	3
Co_9S_8	786	18	$Co_{27}S_{20}$	2230	3
$Co_{10}S_8$	845	10	$Co_{28}S_{19}$	2257	3
$Co_{10}S_9$	877	7	$Co_{28}S_{20}$	2289	5
$Co_{11}S_9$	936	11	$Co_{28}S_{21}$	2321	2
$Co_{12}S_9$	995	10	$Co_{29}S_{20}$	2348	4
$Co_{12}S_{10}$	1027	8	$Co_{29}S_{21}$	2380	3
$Co_{13}S_{10}$	1086	15	$Co_{30}S_{20}$	2407	3
$Co_{13}S_{11}$	1118	4	$Co_{30}S_{21}$	2439	4
$Co_{14}S_{10}$	1145	10	$Co_{31}S_{20}$	2466	2
$Co_{14}S_{11}$	1177	8	$Co_{31}S_{21}$	2498	4
$Co_{14}S_{12}$	1209	4	$Co_{32}S_{21}$	2558	3
$Co_{15}S_{11}$	1236	9	$Co_{32}S_{22}$	2590	3
$Co_{15}S_{12}$	1268	8	$Co_{33}S_{21}$	2617	2
$Co_{16}S_{11}$	1295	4	$Co_{33}S_{22}$	2649	3
$Co_{16}S_{12}$	1327	8	$Co_{33}S_{23}$	2681	2
$Co_{17}S_{12}$	1386	8	$Co_{34}S_{22}$	2708	3
$Co_{17}S_{13}$	1418	4	$Co_{34}S_{23}$	2740	3
$Co_{18}S_{13}$	1477	7	$Co_{35}S_{22}$	2767	1
$Co_{18}S_{14}$	1509	2	$Co_{35}S_{23}$	2799	2
$Co_{19}S_{13}$	1536	6	$Co_{35}S_{24}$	2831	1
$Co_{19}S_{14}$	1568	4	$Co_{36}S_{23}$	2858	3
$Co_{20}S_{13}$	1595	4	$Co_{36}S_{24}$	2890	1
$Co_{20}S_{14}$	1627	6	$Co_{37}S_{23}$	2918	2
$Co_{20}S_{15}$	1658	3	$Co_{37}S_{24}$	2950	3
$Co_{21}S_{14}$	1685	5	$Co_{38}S_{23}$	2977	2
$Co_{21}S_{15}$	1717	4	$Co_{29}S_{20}$	2348	4
$Co_{22}S_{14}$	1744	3			

[a] The assignments of the ions with mass <1780 have been confirmed with high resolution spectra; see text.

$[Fe_7S_6]$ core is characterized in solid-state compounds.[39,40] The $[Fe_7S_7]$ core, like $[Fe_5S_5]$, is an unprecedented stoichiometry in metal chalcogenide cluster chemistry, but **77A** is postulated using the same construction principles, and contains 12 Fe_2S_2 rhombs over its surface. In **77A** three Fe atoms and three S atoms are four-coordinate. By addition of Fe, S, or FeS across the Fe_3S_3 cycles of **66A**, structures **78A** (not shown), **87A** (not shown), and **88A** can be developed. Stereochemical isomers can be envisaged for **88A** according to the number of Fe–Fe bonds involved in the symmetrization. Other structures can be proposed for $[Fe_8S_8]^-$: one, **88B**, with idealized S_4 symmetry, contains an Fe_8 core comprised of two fused trigonal prisms (an unusual octahedron) with S atoms capping the four quadrilateral Fe_4 faces and the four triangular Fe_3 faces. Another structure for $[Fe_8S_8]^-$ is an octagonal prism **88C** (not shown); however, this has fewer Fe–S connections and is not expected to be as stable in the gas phase. So far no M_8S_8 single cluster cores have been established in crystalline materials.

Larger clusters have many possibilities which cannot be discussed fully here. Structures generated by addition to **88A** are generally surface crowded, but the polyhedral connectivity of **88A** can be expanded in structures such as **1010A**. An alternative structural principle of stacked M_3S_3 triangular planes embodied in **99A** has direct precedent in $[Ni_9S_9(PEt_3)_6]^{2+}$ [42] and is known in other nickel,[43] cobalt,[44] and molybdenum[45] chalcogenide clusters. Contracted structures such as **99A** and polyhedral structures such as **1010A** differ fundamentally in the number of short bonding interactions through the center, a distinction to be assessed by further calculations. A structure to be investigated for $[Fe_{11}S_{10}]^-$ is the **1010A** cage with a central Fe atom, and for clusters beyond this size it is possible to envisage structures based on an Fe core coated by a shell composed principally of Fe_2S_2 rhombs. However, without observations of $[Fe_xS_y]^-$ ions with $x > 11$, we do not know how x becomes progressively greater than y as x increases, as expected for larger $[Fe_xS_y]^-$ ions with an Fe core plus an FeS coating; this data is available for the $[Co_xS_y]^-$ ions.

Structural Features for $[Fe_nS_{n+5}]^-$ and $[Fe_nS_{n+6}]^-$ Ions. This well-defined series of ions signifies the existence of a structural principle for stable ions: what is it? The simplest structural interpretation involves addition of S_5 to the globular clusters of series a, increasing the coordination of the surface Fe atoms. This can be done in various ways, including chelation at one Fe atom, connection from one Fe to another, and bridging from one Fe_2 pair to another. Structure **1** shows some of the modes of connection

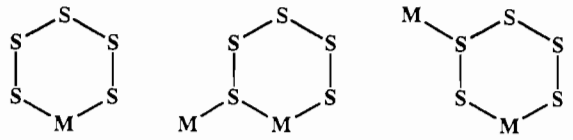

1

between a polysulfide ion and a metal atom, for which there is precedent in crystal structures.[31c] The unanswered question in this interpretation is why there is only one S_5 additional for each Fe_n: in order to increase the coordination at all Fe atoms in each cluster more than one S_5 would be required. There is substantial precedent for S_2 and S_3 groups coordinated to Fe in crystals, but if such groups occurred in the gaseous clusters formed in our experiments we would expect that the ion compositions would vary by S_2 or S_3 increments, which is not observed. An alternative structural principle involves elongated structures. There is now evidence for two types of extended structure, one (**2**) with a single

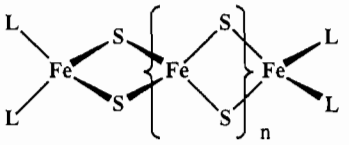

2

chain of bridged Fe atoms, the other (**3**) with a double chain or

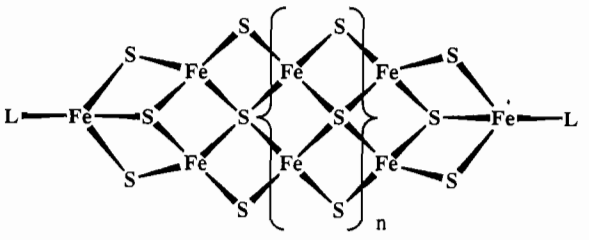

3

ribbon. The precedence for structure type **2** is in the compounds

(42) Cecconi, F.; Ghilardi, C. A.; Midollini, S. *Inorg. Chem.* **1983**, *22*, 3802–3808.

(43) (a) Fenske, D.; Ohmer, J. *Angew. Chem. Int. Ed. Engl.* **1987**, *26*, 148–150. (b) Hong, M.; Huang, Z.; Liu, H. *J. Chem. Soc., Chem. Commun.* **1990**, 1210–1211.

(44) Fenske, D.; Ohmer, J.; Hachgenei, J. *Angew. Chem., Int. Ed. Engl.* **1985**, *24*, 993–995.

(45) Gougeon, P.; Potel, M.; Sergent, M. *Acta Crystallogr.* **1990**, *C46*, 2284–2287.

Table III. Negative Ions and Neutrals Formed by Collisional Activation

parent ion	major or first daughter ions	neutral fragments lost	minor ions (neutrals lost)	other ions formed after long periods
$[Fe_2S_3]^-$	$[FeS_2]^-$	FeS		$[S]^-$, $[FeS_3]^-$
$[Fe_3S_3]^-$	$[Fe_2S_3]^-$	Fe	$[FeS_2]^-$ (Fe_2S)	$[S]^-$
$[Fe_3S_4]^-$	$[Fe_3S_3]^-$	S	$[S]^-$ (Fe_3S_3), $[Fe_2S_3]^-$ (FeS_2)	$[S_3]^-$
$[Fe_4S_5]$	$[FeS_2]^-$	Fe_3S_3		
$[Fe_5S_6]^-$	$[Fe_4S_5]^-$, $[FeS_2]^-$	FeS, Fe_4S_4	$[Fe_3S_3]^-$ (Fe_2S_3)	$[Fe_3S_4]^-$, $[Fe_2S_3]^-$
$[Fe_6S_6]^-$			$[Fe_3S_3]^-$ (Fe_3S_3), $[Fe_5S_6]^-$ (Fe), $[Fe_4S_5]^-$ (Fe_2S)	$[Fe_3S_4]^-$, $[FeS]^-$, $[S]^-$, $[S_3]^-$, $[S_4]^-$
$[FeS_6]^-$	$[FeS_4]^-$	S_2		
$[FeS_7]^-$	$[FeS_5]^-$	S_2		
$[CoS_2]^-$ [a]	$[S]^-$	CoS		
$[Co_2S_3]^-$ [a]	$[CoS_2]^-$	CoS	$[CoS_3]^-$ (Co)	
$[Co_3S_3]^-$ [a]	$[Co_2S_3]^-$	Co	$[Co_2S_2]^-$ (CoS)	
$[Co_4S_4]^-$	$[Co_3S_3]^-$	CoS	$[Co_4S_2]^-$ (S_2)	$[CoS_2]^-$, $[CoS_3]^-$, $[Co_2S_3]^-$
$[Co_5S_4]^-$	$[Co_3S_3]^-$	Co_2S	$[Co_4S_4]^-$ (Co)	$[Co_2S_3]^-$, $[Co_4S_2]^-$, $[Co_4S_5]^-$
$[Co_5S_5]^-$	stable			
$[Co_6S_6]^-$	$[Co_3S_3]^-$, $[Co_2S_2]^-$	Co_3S_3, Co_4S_4	$[Co_6S_4]^-$ (S_2)	$[Co_4S_4]^-$, $[Co_6S_5]^-$, $[CoS_2]^-$
$[Co_7S_6]^-$	$[Co_3S_3]^-$, $[Co_7S_5]^-$	Co_4S_3, Co	$[Co_6S_6]^-$ (Co), $[Co_6S_4]^-$ (CoS_2)	
$[Co_8S_7]^-$	$[Co_7S_6]^-$	CoS	$[Co_8S_6]^-$ (S), $[Co_6S_6]^-$ (Co_2S), $[Co_6S_4]^-$ (Co_2S_3)	$[Co_3S_3]^-$, $[Co_4S_2]^-$, $[Co_5S_5]^-$
$[Co_9S_8]^-$	$[Co_9S_7]^-$, $[Co_8S_5]^-$	S, CoS_3	$[Co_7S_7]^-$ (Co_2S)	$[Co_7S_6]^-$, $[Co_3S_3]^-$, $[Co_8S_7]^-$, $[Co_9S_6]^-$

[a] Stable ion with very little collisionally activated dissociation.

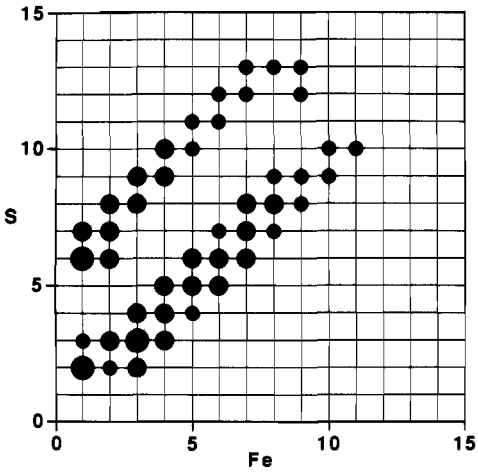

Figure 3. Map of the compositions of the observed ions $[Fe_xS_y]^-$, with relative intensity indicated by the size of the circle. Series a and b described in the text are bottom and top, respectively.

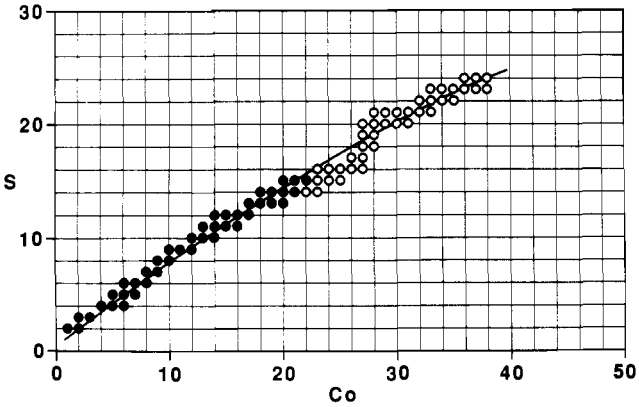

Figure 4. Map of the compositions of the observed ions $[Co_xS_y]^-$. Compositions marked as open circles have not been confirmed by high resolution spectra.

$[Fe_4S_6(SEt)_4]^{4-}$, $[Fe_5S_8(SEt)_4]^{5-}$, and $[Fe_6S_{10}(SEt)_4]^{6-}$,[46a] while the established compounds $[Fe_6S_9(SR)_2]^{4-}$ [39] and $[Fe_8S_{12}(SR)_2]^{4-}$ [46] are the first members of the series **3**. The structural features of **2** and **3** are present in the cyclic and bicyclic molecules $[Na_2Fe_{18}S_{30}]^{8-}$ and $[Na_9Fe_{20}Se_{38}]^{9-}$.[36] The postulated structures are then as follows: $[Fe_3S_8]^-$ (**2**), $n = 1$, four L = S; $[Fe_4S_9]^-$ (**3**), $n = 0$, both terminal FeL void; $[Fe_4S_{10}]^-$ (**2**), $n = 2$, four L = S; $[Fe_5S_{10}]^-$ (**2**), $n = 3$, two L = S, two L void; $[Fe_5S_{10}]^-$ (**3**), $n = 0$, one terminal FeL void, one L = S; $[Fe_5S_{11}]^-$ (**2**), $n = 3$, three L = S, one L void; $[Fe_6S_{11}]^-$ (**3**), $n = 0$, both L = S; $[Fe_6S_{12}]^-$ (**2**), $n = 4$, two L = S, two L void; $[Fe_7S_{12}]^-$ (**2**), $n = 5$, four L void; $[Fe_7S_{13}]^-$ (**2**), $n = 5$, one L = S, three L void; $[Fe_7S_{13}]^-$ (**3**), $n = 1$, one L = S, one FeL void; $[Fe_8S_{13}]^-$ (**3**), $n = 1$, one L = S, one L void. We note that the ions $[FeS_6]^-$, $[FeS_7]^-$, $[Fe_2S_7]^-$, $[Fe_2S_8]^-$, and $[Fe_3S_9]^-$ cannot be modeled by **2** or **3**.

The ion $[Fe_2S_6]^-$ can be described as **2** with $n = 0$ and four L = S, while the ions $[Fe_9S_{12}]^-$ and $[Fe_9S_{13}]^-$, which also do not fit the $[Fe_nS_{n+5}]^-$ or $[Fe_nS_{n+5}]^-$ series, cannot be accommodated by models **2** or **3**.

We note that other precedented structure types with terminal Fe–S can be postulated, such as cyclic $[(\mu\text{-}S)_3(FeS_2)_3]$ for $[Fe_3S_9]^-$ and the adamantanoid cage structure $[(\mu\text{-}S)_6(FeS)_4]$ for $[Fe_4S_{10}]^-$. Refinement of the various postulates for the series b ions will depend on calculations of electronic structure, in progress.

Expected Structural Features for $[Co_xS_y]^-$ Ions. There are many possibilities for the structures of the large number of $[Co_xS_y]^-$ ions. We will describe here only a few key structures which we believe to demonstrate the relevant principles and postulate that intermediate ions will have intermediate structures. We will discuss structural models in more detail in a separate publication. Many of the ions up to $[Co_{10}S_9]^-$ have the same compositions as those already described for iron, and therefore inherit the same structural possibilities. Precedent for structures **44A** and **76A** exists in the cobalt compounds $[Co_4S_4(Ph_3P)_4]$,[44] $[Co_7S_6Cl_2(Ph_3P)_5]$,[47a] $[Co_7S_6Cl_{1.5}Br_{1.5}(Ph_3P)_4]$,[47b] and $[Co_7S_6I_3(PEt_3)_4]$.[47c] However, the measured dissociations of the $[Co_xS_y]^-$ and corresponding $[Fe_xS_y]^-$ ions are generally different (see Table III), as would be expected due to bonding differences, and we comment on the possible structural implications of this. It is significant that Co_3S_3 occurs as the most intense anion in the laser ablation spectrum and frequently as anion and neutral in the dissociation of larger ions. The dissociation of structure **44A** (for $[Co_4S_4]^-$) by loss of one edge of the cube would yield structure

(46) (a) Al-Ahmad, S. A.; Kampf, J. W.; Dunham, R. W.; Coucouvanis, D. *Inorg. Chem.* **1991**, *30*, 1163. (b) Coucouvanis, D. Personal communication.

(47) (a) Fenske, D.; Hachgenei, J.; Ohmer, J. *Angew. Chem., Int. Ed. Engl.* **1985**, *24*, 706–709. (b) Jiang, F.; Huang, L.; Lei, X.; Liu, H.; Kang, B.; Huang, Z.; Hong, M. *Polyhedron* **1992**, *11*, 361–363. (c) Cecconi, F.; Ghilardi, C. A.; Midollini, S.; Orlandini, A. *Inorg. Chim. Acta* **1991**, *184*, 141–145.

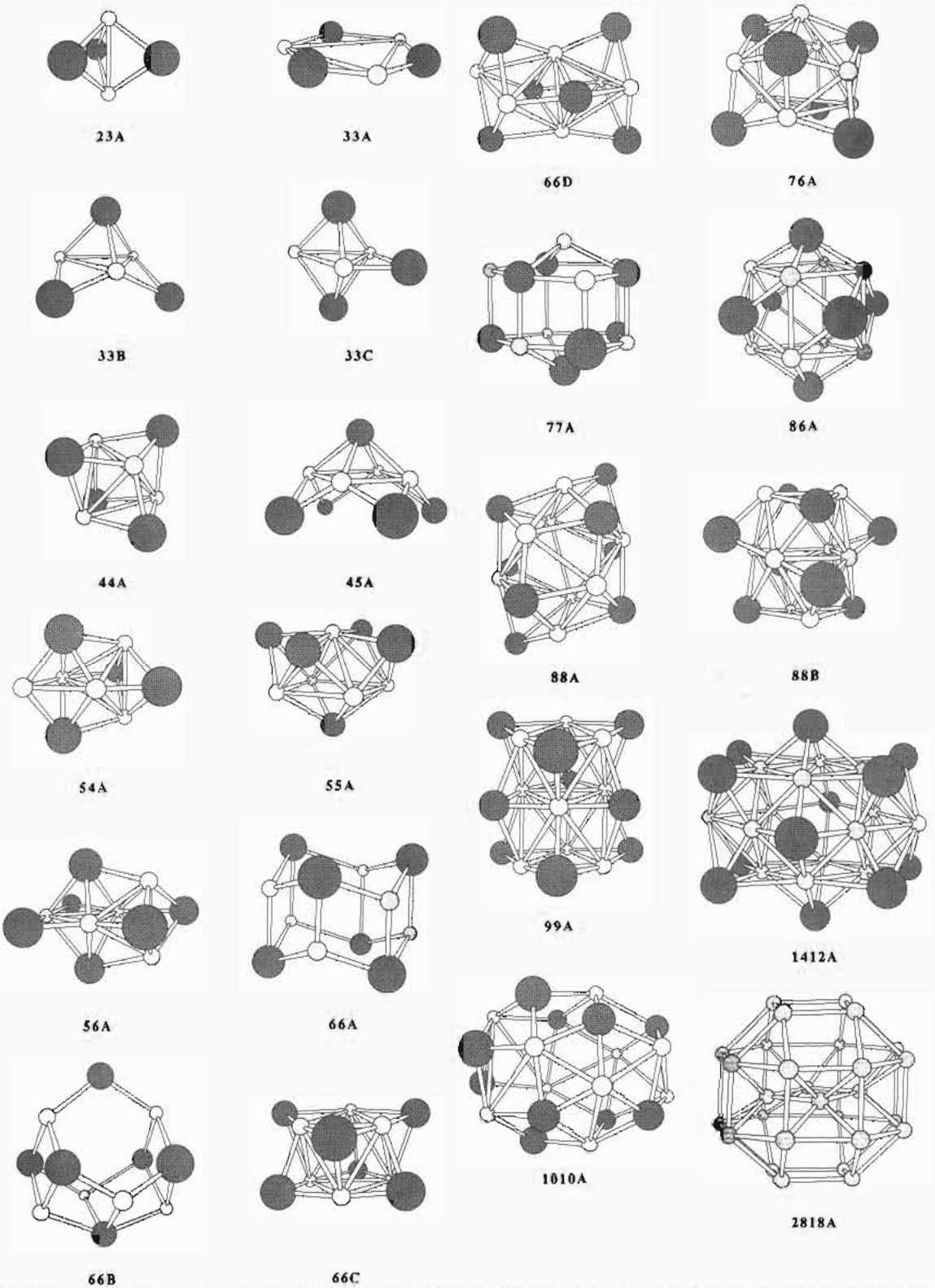

Figure 5. Some of the postulated structures for $[M_xS_y]$ clusters, labelled *xy*X (X = A, B, ...). M–S bonds (ca. 2.2 Å) are shown, and probable M–M bonding interactions (ca. 2.6 Å) are marked. See text about **2818A**.

33B. The ion $[Co_4S_2]^-$ occurs as the dissociation product of $[Co_4S_4]^-$, $[Co_5S_4]^-$, and $[Co_8S_7]^-$: a possible structure is the pseudooctahedral $(\mu_4\text{-S})_2Co_4$. While the dissociation of a Co atom from structure **54A** (for $[Co_5S_4]^-$) can obviously yield structure **44A**, there are several ways for a Co_2S triangle to dissociate from structure **54A** to yield **33B** or **33C**. $[Co_5S_5]^-$ appears to be a particularly stable ion, consistent with structure **55A**. $[Co_6S_4]^-$ is both a primary ion in the laser ablation and a dissociation product, and a high-symmetry structure composed of an M_6 octahedron capped with μ_3-S on four faces is postulated. The dissociation of $[Co_6S_6]^-$ to $[Co_3S_3]^-$ plus Co_3S_3 is consistent with the 3-fold structures **66A** and **66C**, while the dissociation of $[Co_6S_6]^-$ to $[Co_2S_2]^-$ plus Co_4S_4 is more consistent with structure **66D**. Although structure **66B** could be invoked to account for the formation of $[Co_6S_5]^-$ plus S after long periods, it is not generally supported by the behavior of $[Co_6S_6]^-$. Structure **76A** for $[Co_7S_6]^-$ has strong precedent in crystalline compounds: the initial fragmentation to $[Co_3S_3]^-$ plus Co_4S_3 would involve considerable bond-breaking, while the fragmentation to $[Co_6S_6]^-$ plus Co is readily described. For $[Co_8S_6]^-$, which occurs as both

a primary ion and a dissociation product, the high-symmetry **86A** structure is well-established in the core of $[Co_8S_6(SPh)_8]^{4-}$.[48]

The fact that y becomes progressively less than x as x increases in the $[Co_xS_y]^-$ ions indicates that the structural type will progress toward a core of Co atoms, with the S atoms capping faces. An illustration of this structure type is the postulate **1412A**, which can be understood as a hexa-Co-capped inner cube Co_8, with S atoms capping all of the Co_4 surface faces. The ion $[Co_{15}S_{12}]^-$ could have the same structure but with Co at the center. For $[Co_xS_y]^-$ ions larger than $[Co_{15}S_{12}]^-$, increasing numbers of Co atoms can be accommodated within a cobalt polyhedral core. This principle accounts for the curvature in the Co_xS_y ion map, which becomes more pronounced as x increases above 16. An illustration of such a core structure type is shown in diagram **2818A** (on which the S atoms are omitted). The Co_{28} core is composed of 24 outer Co atoms, arranged as layers of four, eight, eight, and four, and four inner Co atoms. There are 18 square faces on the surface of this core, which are proposed as the locations of the μ_4-S atoms. This structural principle has precedent in the crystal structure of $Ni_{34}Se_{22}(PPh_3)_{12}$,[44] in which the Ni core has layers of five, ten, ten, and five Ni atoms enclosing another four Ni atoms, and with the Se atoms capping the quadrilateral and pentagonal faces of the Ni_{34} core. We observe a considerable number of $[Co_xS_y]^-$ ions with $32 \leq x, \leq 38$ and $21 \leq y \leq 24$, and it is postulated that they all have structures closely similar to that of the core of $Ni_{34}Se_{22}(PPh_3)_{12}$.

Electronic Structure. Although the electronic structures for these clusters await definitive calculation, a comparative analysis of the electron populations in the clusters $[M_xS_y]^-$ for the four metals Fe, Co, Ni, and Cu is possible, and the bonding notions implicit in the foregoing discussion of geometric structure can be developed in broad terms. However, the specific relationships between electron populations and geometrical structure that have been developed for metal clusters[49-52] are not directly applicable to metal chalcogenide clusters, because the electron contributions from the group 16 atoms vary with bonding mode,[53] and each chalcogen atom increments the total by more than two electrons.[27] We draw attention to the following patterns, to be investigated further by more substantial theory.

Figures 6 and 7 show the ion maps for $[Ni_xS_y]^-$ (ex Ni_2S_3) and $[Cu_xS_y]^-$ (ex KCu_3S_4) respectively, for comparison with Figures 3 and 4 for Fe and Co. The general slopes (x/y) of the ion distributions correlate with the electron population of the metal, in the sense that the M/S ratio increases as the electron population of the metal increases. The ion map of FeS (disregarding the polysulfide ions) has a M/S slope of 1 and the ions $[Fe_xS_y]^-$ with $x = y$ are generally the most abundant. The slopes of the ions produced by the other metals increase, up to $x/y = 1.9$ for $[Cu_xS_y]^-$, as shown in Figures 3–6. This regular increase with metal atomic number signifies a dependence of composition, and thus geometry and bonding, on the number of electrons in the cluster.

For example, if we sum the 3d and 4s electrons of the metal atoms and add six electrons for each sulfur atom and one electron for the charge, and divide by the number of metal atoms we get N_m, the number of electrons per metal atom. Representative N_m values are listed in Table IV, arranged according to the number

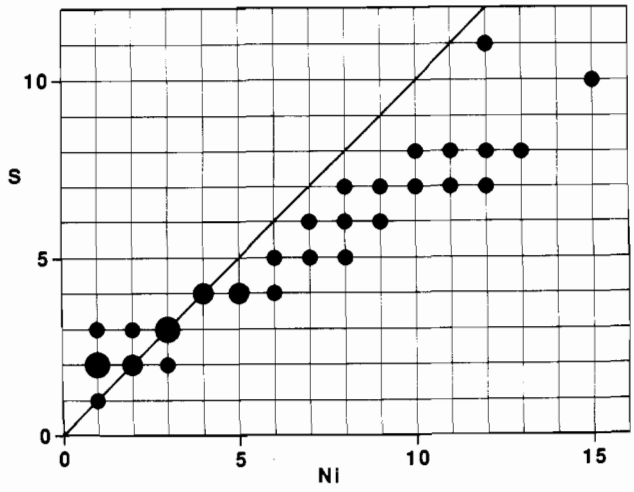

Figure 6. Map of the compositions of the observed ions $[Ni_xS_y]^-$, with relative intensity indicated by the size of the circle.

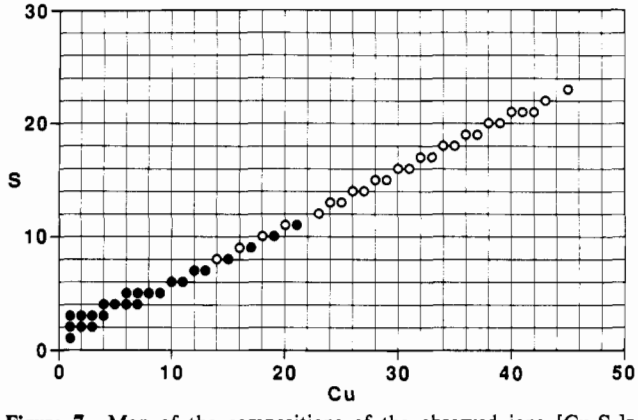

Figure 7. Map of the compositions of the observed ions $[Cu_xS_y]^-$. Compositions marked as open circles have not been confirmed by high resolution spectra.

of metal atoms per cluster; where there is a choice of y, the most abundant ion is calculated. Also included in Table IV are corresponding data for selected $[Mn_xS_y]^-$ ions.[54] There are two interesting and general results from the table.

(A) In any row (constant number of metal atoms) the electron populations N_m tend to be largely independent of the identity of the metal. This independence is most apparent in the larger ions, where the quantized values of y/x and thus of N_m are closer together.

(B) The electron population per metal decreases regularly as the size of the cluster increases, from $N_m \sim 15$ when $x = 5$, to $N_m \sim 14$ when $x = 12$, to about $N_m \sim 12.5$ for clusters with 37 metal atoms. This trend is apparent in the curvature of the $[Co_xS_y]^-$ ion map (Figure 4), with x/y increasing (toward the slope for Cu, Figure 6) as x increases.

While the concept of metal-independent electron population in metal clusters underlies most qualitative theories, it had not previously been recognized in extended series of metal chalcogenide clusters. While electron counting rules are usually precise for clusters with no ligands or two-electron ligands, the consistency of the values in the rows of Table IV is slightly surprising because the increment in electron counting is six. Given the wide range of ion compositions from Mn to Cu, for example the Mn_{12} cluster has S_{13} while the Cu_{12} cluster has S_7, it might have been expected that different patterns of electronic structure would be involved because different geometrical structures are necessitated by the stoichiometry differences. While the cluster orbitals will have increasing metal character across the transition series (necessitated

(48) Christou, G.; Hagen, K. S.; Bashkin, J. K.; Holm, R. H. *Inorg. Chem.* **1985**, *24*, 1010–1018.
(49) (a) Lauher, J. W. *J. Am. Chem. Soc.* **1978**, *100*, 5305–5315. (b) Lauher, J. W. *J. Am. Chem. Soc.* **1979**, *101*, 2604.
(50) (a) Mingos, D. M. P. *Acc. Chem. Res.* **1984**, *17*, 311–9. (b) Mingos, D. M. P.; Johnston, R. L. *Struct. Bonding* **1987**, *68*, 29–87. (c) Mingos, D. M. P.; Slee, T.; Zhenyang, L. *Chem. Rev.* **1990**, *90*, 383–402. (d) Wales, D. J.; Mingos, D. M. P.; Slee, T.; Zhenyang, L. *Acc. Chem. Res.* **1990**, *23*, 17–22.
(51) Owen, S. M. *Polyhedron* **1988**, *7*, 253.
(52) Teo, B. K.; Zhang, H. *J. Cluster Sci.* **1990**, *1*, 155 and references cited therein.
(53) Wheeler, R. A. *J. Am. Chem. Soc.* **1990**, *112*, 8737–8741.
(54) Dance, I. G.; Fisher, K. J.; Willett, G. D. Manuscript in preparation.

Table IV. Number of Electrons per Metal, N_m[a]

Mn[b]		Fe		Co		Ni		Cu	
ion	N_m	ion	N_m	ion	N_m	ion	N_m	ion	N_m
$[Mn_4S_5]^-$	14.8	$[Fe_4S_4]^-$	14.3	$[Co_4S_4]^-$	15.3	$[Ni_4S_4]^-$	16.3	$[Cu_4S_3]^-$	15.8
		$[Fe_5S_5]^-$	15.6	$[Co_5S_4]^-$	15.0				
		$[Fe_6S_7]^-$	15.2	$[Co_6S_6]^-$	15.2	$[Ni_6S_4]^-$	14.0		
		$[Fe_9S_9]^-$	14.1	$[Co_9S_8]^-$	14.4	$[Ni_9S_6]^-$	14.1	$[Cu_9S_5]^-$	14.4
$[Mn_{10}S_{11}]^-$	13.7	$[Fe_{10}S_9]^-$	13.5	$[Co_{10}S_8]^-$	13.9	$[Ni_{10}S_7]^-$	14.3	$[Cu_{10}S_6]^-$	14.7
$[Mn_{12}S_{13}]^-$	13.8			$[Co_{12}S_9]^-$	13.8	$[Ni_{12}S_8]^-$	14.0	$[Cu_{12}S_7]^-$	14.6
				$[Co_{15}S_{12}]^-$	13.8	$[Ni_{15}S_{10}]^-$	14.1	$[Cu_{15}S_8]^-$	14.3
				$[Co_{23}S_{16}]^-$	13.2			$[Cu_{23}S_{12}]^-$	14.2
				$[Co_{37}S_{24}]^-$	12.9			$[Cu_{37}S_{19}]^-$	12.1

[a] See text for definition and method of calculation. [b] Fisher, K. J.; Dance, I. G.; Willett, G. D. To be published.

by the decreasing number of sulfur atoms and orbitals), their populations are largely independent of metal identity. Superimposed on this general picture are smaller variations in the electronic structure patterns (the ion maps have different detailed features) due the differing numbers of sulfur atoms and different (metal dependent) utilization of M–S bonding geometries.

Trend B, namely decreasing values of N_m as the size (x) of the cluster increases, reflects the increase in the proportion of M–M bonds as size increases. Reduction in N_m is compensated because homoatomic M–M bonding increases the formal electron population at each M atom, as in metal clusters with other ligands. The trend in the N_m values with size increase is equivalent to a variation between 18 electron population for the metal when $x = 1$ to the electron population of the bulk metal as $x \rightarrow \infty$. The geometrical postulates made above are entirely consistent with this conclusion from electron populations; the larger clusters concentrate M atoms and M–M bonding inside the cluster, with M–S bonding on the periphery.

Conclusions

Laser ablation of metal chalcogenides, coupled with Fourier transform mass spectrometry, can generate and examine metal chalcogenide cluster anions larger and more numerous than those which have been characterized in crystals. These gaseous clusters approach the size regime of synthetic metal chalcogenide colloids[3,6a] and the bionanoclusters of CdS.[8] The larger gaseous clusters (at least of Co and Cu) do not have an even distribution of M and S atoms throughout and are not homogeneous fragments of nonmolecular metal chalcogenide lattices. The concentration of metal atoms inside the larger chalcogenide clusters of iron, cobalt, nickel, and copper is supported by the crystal structures of $[Cu_{29}Se_{15}(PPr^i_3)_{12}]$, $[Cu_{30}Se_{15}(PPr^i_3)_{12}]$, $[Ni_{34}Se_{22}(PPh_3)_{12}]$,[44] $[Cu_{36}Se_{18}(PBu^t_3)_{12}]$,[55] and $[Cu_{70}Se_{35}(PEt_3)_{22}]$.[56] There is a significant difference between these gas phase clusters $[M_xS_y]^-$ and nanoclusters of CdS, in that all evidence indicates that the latter are structural fragments of nonmolecular lattices.[3,57]

Finally we observe that despite the substantial range of metal chalcogenide cluster cores now characterized in crystalline compounds, the results reported here presage the stability and possible existence of metal chalcogenide clusters (with appropriately terminal ligation) having compositions and sizes far beyond previous expectations. We note that in general the known $M_xS_yL_z$ clusters (with L usually phosphine or halide) do correspond in core composition to the $[M_xS_y]^-$ clusters observed in the gas phase, providing further support to the possibility of stabilizing the gaseous clusters with appropriate terminal ligands. These exciting prospects are directing our further work, encompassing the ab initio calculation of electronic structure for M_xS_y clusters and the synthesis of additional clusters by conventional methods or by condensation from the gas phase.

Acknowledgment. This research is funded by the Australian Research Council. K.J.F. gratefully acknowledges a National Research Fellowship, and J.E.N. an Australian Postgraduate Award. We thank Professor D. Coucouvanis for providing unpublished information and a reviewer for helpful comments.

(55) Fenske, D.; Krautscheid, H.; Balter, S. *Angew. Chem., Int. Ed. Engl.* **1990**, *29*, 796–799.
(56) Fenske, D.; Krautscheid, H. *Angew. Chem., Int. Ed. Engl.* **1990**, *29*, 1452.
(57) Marcus, M. A.; Flood, W.; Stiegerwald, M.; Brus, L.; Bawendi, M. *J. Phys. Chem.* **1991**, *95*, 1572.